Resonant Raman scattering in a magnetic field assisted by Fröhlich interaction in zinc-blende-type semiconductors

V. López-Richard* and G. E. Marques
Departamento de Física, Universidade Federal de São Carlos, 13566-905, São Carlos, SP, Brazil

C. Trallero-Giner and J. Drake
Departamento de Física Teórica, Universidad de La Habana, 10400 C. Habana, Cuba

(Received 9 April 1998)

The Raman profiles are calculated as a function of magnetic field B_0 and the laser frequency ω_L for the Fröhlich type of electron-phonon interaction in parallel scattering configurations with circularly polarized light $[\overline{z}(\sigma^{\pm},\sigma^{\pm})z]$ spread in z along the [001] crystal direction. A 4×4 Luttinger Hamiltonian has been used in order to take the valence-band admixture into account. Explicit expressions for the Raman scattering efficiency as a function of ω_L, B_0, and the Luttinger parameters are given. Different effects due to the band nonparabolicity and the mixing of valence-band states are discussed. For a realistic picture of the resonance profiles an explicit calculation of the lifetime broadening of the intermediate electronic states assisted by a LO phonon has been carried out including the dependence on the laser incident energy, magnetic field, and Landau quantum number. Results are applied to explain recent experimental data for GaAs. [S0163-1829(98)06948-3]

I. INTRODUCTION

By studying the behavior of the Raman intensity as a function of an applied magnetic field in polar semiconductors one is able to observe strong resonances appearing near the critical points in the density of states. The Raman intensity dependence on the laser energy provides information about the characteristics of the crystal band structure, and the selection rules involved in these processes show the relation between the polarization of the incident and scattered lights and the symmetry properties of the induced excitations. Using different scattering configurations in zinc-blende-type semiconductors one may separate the contributions from the electron-phonon interaction via deformation potential or Fröhlich Hamiltonian.[1–4]

In the Faraday backscattering configuration, with parallel incident and scattered circular polarization and z along the [001] crystal direction $[\overline{z}(\sigma^{\pm},\sigma^{\pm})z]$, the electron-phonon coupling occurs via the Fröhlich-like interaction. This kind of first-order Raman scattering is associated with dipole-forbidden processes and the scattering intensities, out of resonance, are much weaker if compared to those obtained in the deformation potential case.[3]

In this work we develop a theoretical model that takes into account the valence-band mixing and the lifetime level broadening in order to describe the one-phonon magneto-Raman resonances due to transitions assisted by the Fröhlich interaction. The energy broadening in the magnetoresonance line shape is calculated by introducing the dependence on Landau-level indexes, laser frequency, and magnetic-field strength. The enhancement of the electron (hole) lifetime broadening due to the electron-phonon Fröhlich coupling strongly modifies the magneto-Raman profiles. The Raman spectra present interesting dependences of the energy broadening on the Landau-level indexes and the electron (hole) wave vector. The differences between the Luttinger and simple parabolic models, together with the effects of the valence-band admixture, are also analyzed. Several transitions appearing in the present model cannot be predicted in the three-band parabolic approximation. The valence-band admixture also provides the necessary conditions for the existence of double resonances; however, as will be shown later, this effect is, in general, too weak to be observed experimentally.

The magnetopolaron effects, produced by the electron-phonon Fröhlich interaction and the magnetic-field strength may also change the shape and the linewidth of the electronic states. As already observed, this coupling introduces a change in the self-energy of the electronic states[5–7] due to the emission and absorption of virtual phonons that become resonant at certain critical values of the applied magnetic field and yielding anticrossings in the former Landau-level ladder. In Refs. 6 and 7, the magnetopolaron effect in one-phonon resonant Raman scattering was discussed in the framework of a two-band model. Following the procedure of Ref. 5 the magnetopolaron effects are also analyzed in the context of the present work and some features that appear in the available GaAs Raman experimental data are explained.

The paper is organized as follows. In Sec. II we summarize the Hamiltonian model and the corresponding solutions for the electronic states in the valence and conduction bands, following the procedures already reported in Ref. 3. The expressions for the scattering amplitudes in the Faraday scattering configuration are obtained in Sec. III. Section IV is devoted to the discussion of the electron-hole self-energy and the band admixture on the magneto-Raman efficiency. A direct comparison with recent experimental results is presented. Finally, in Sec. V we summarize our main results.

II. BASIC HAMILTONIAN AND WAVE FUNCTIONS

The Luttinger-Kohn Hamiltonian model[8,9] provides a good description for the electronic states in semiconductors where the spin-orbit and the band-gap energies are large (say, E_g, $\Delta_0 \geqslant 300$ meV). In this case the 8×8 Kane-Weiller Hamiltonian[10] can be separated into two 2×2 matrices for Γ_6^c conduction (cc) and Γ_7^{so} split-off (so) bands, or the so-

called parabolic models, and a 4×4 matrix for heavy-hole (hh) and light-hole (lh) states, or the well-known Luttinger Hamiltonian model for the Γ_8^v symmetry valence-band states.[9] The coupling between hh and lh ladders due to the Γ_8^v degeneracy is included through this 4×4 Hamiltonian model (H_{vv}). Schematically the full Hamiltonian can be written as

$$\hat{H}=\begin{bmatrix} H_{cc} & 0 & 0 \\ 0 & H_{vv} & 0 \\ 0 & 0 & H_{ss} \end{bmatrix}, \tag{1}$$

with

$$H_{cc}=E_g+\frac{\hbar^2\hat{\mathbf{k}}^2}{2m_c}+\tfrac{1}{2}\,g_c\mu_B\boldsymbol{\sigma}\cdot\mathbf{B}, \tag{2}$$

$$H_{ss}=-\Delta_0-\frac{\hbar^2\hat{\mathbf{k}}^2}{2m_{so}}+\tfrac{1}{2}\,g_{so}\mu_B\boldsymbol{\sigma}\cdot\mathbf{B}, \tag{3}$$

and

$$\begin{aligned} H_{vv}=&-\frac{\hbar^2}{2m_0}\{\gamma_1\hat{\mathbf{k}}^2+\gamma_2[(\tfrac{1}{3}J^2-J_x^2)\hat{k}_x^2+\text{c.p.}] \\ &-4\gamma_3[\{J_xJ_y\}\{\hat{k}_x\hat{k}_y\}+\text{c.p.}] \\ &+2\kappa\,\mu_B J_z B_0+2q_{LK}J_z^3 B_0\}, \end{aligned} \tag{4}$$

where c.p. stands for cyclic permutations, μ_B is the Bohr magneton, σ is the Pauli matrix, γ_1, γ_2, γ_3, κ, q_{LK} are the Luttinger parameters, J_i $(i=x,y,z)$ are the angular momentum matrices, E_g and Δ_0 are the energy gap and spin-orbit splitting, respectively. Also, m_c (m_{so}), g_c (g_{so}) are the effective mass and g-Landé factor of conduction (splitoff) band, respectively. The magnetic interaction is included in the wave-vector operator $\hat{\mathbf{k}}=-i\nabla+(e/c\hbar)\,\mathbf{A}$.

We consider the system subjected to a homogeneous magnetic field $\mathbf{B}$ parallel to the z axis where the Landau gauge $\mathbf{A}=(0,xB_0,0)$ for the vector potential is chosen. The eigenfunctions and eigenvalues for the $\{\Gamma_6^c,\Gamma_7^{so}\}$ manifolds described by Eqs. (2) and (3) can be found elsewhere.[3,9] The analytical solutions of the Schrödinger equation for the Γ_8^v band can be obtained if no warping effect ($q_{LK}\simeq0$) is considered and the axial approximation ($\gamma_2\simeq\gamma_3$) is taken into account. The exact eigensolutions are

$$\begin{aligned} \Psi_1=&a_{11}(N,k_z)|N-2;\tfrac{3}{2},\tfrac{3}{2}\rangle+a_{21}(N,k_z) \\ &\times|N;\tfrac{3}{2},-\tfrac{1}{2}\rangle\overset{x\to\infty}{\longrightarrow}|N;\mathrm{lh}^-\rangle, \end{aligned} \tag{5}$$

$$\begin{aligned} \Psi_2=&a_{12}(N,k_z)|N-2;\tfrac{3}{2},\tfrac{3}{2}\rangle+a_{22}(N,k_z) \\ &\times|N;\tfrac{3}{2},-\tfrac{1}{2}\rangle\overset{x\to\infty}{\longrightarrow}|N-2;\mathrm{hh}^+\rangle, \end{aligned} \tag{6}$$

$$\begin{aligned} \Psi_3=&a_{13}(N,k_z)|N-2;\tfrac{3}{2},\tfrac{1}{2}\rangle+a_{23}(N,k_z) \\ &\times|N;\tfrac{3}{2},-\tfrac{3}{2}\rangle\overset{x\to\infty}{\longrightarrow}|N-2;\mathrm{lh}^+\rangle, \end{aligned} \tag{7}$$

$$\begin{aligned} \Psi_4=&a_{14}(N,k_z)|N-2;\tfrac{3}{2},\tfrac{1}{2}\rangle+a_{24}(N,k_z) \\ &\times|N;\tfrac{3}{2},-\tfrac{3}{2}\rangle\overset{x\to\infty}{\longrightarrow}|N;\mathrm{hh}^-\rangle, \end{aligned} \tag{8}$$

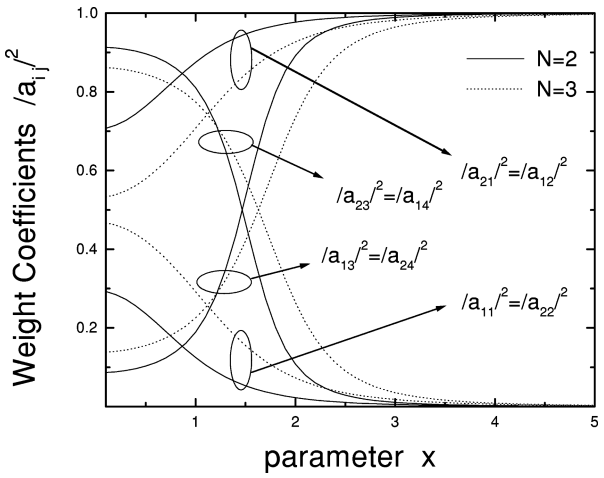

FIG. 1. Weight coefficients $|a_{ij}|^2$ of the admixed wave functions $|\Psi_j\rangle$ calculated as a function of $x=\sqrt{\hbar k_z^2/(2m_0\omega_c)}$, for different Landau quantum numbers: $N=2$ (solid line), $N=3$ (dashed line).

where $a_{ij}(N,k_z)$ is already defined in Eqs. (15)–(18) of Ref. 3.

A quantitative idea about the mixing between the Γ_8^v valence bands is presented in Fig. 1, where the weight factors $|a_{ij}|^2$ $(i=1,2;\ j=1,2,3,4)$, for different Landau levels N, are shown as a function of dimensionless parameter $x=\sqrt{\hbar k_z^2/(2m_0\omega_c)}$. The parameter x is a measure of the ratio between the kinetic energy for the motion along the magnetic field and the cyclotron energy of the motion in the plane perpendicular to the magnetic field. Here, $\omega_c=(eB_0/cm_0)$ is the bare electron cyclotron frequency. In the limit $x\to\infty$ and for Landau quantum number $N>2$, pure heavy- or light-hole states are obtained, thus in this limit the carrier effective masses are constant. This model has been considered in Ref. 2 to evaluate the one-phonon resonant Raman scattering in III-V semiconductors. However, for low values of x the characters of the states appear to be very admixed. Even a change in the character of the state may occur for small values of x, as, for instance, those described by the functions Ψ_3 and Ψ_4 in the $x\to\infty$ and $x\sim0$ cases. Notice that Ψ_3 is a pure lh^+ state in the parabolic limit but its character changes to an almost pure hh^- state for $x\sim0$ (see in Fig. 1 the behavior of a_{13} and a_{23} as functions of x). Similarly, the eigenstates described by functions Ψ_1 and Ψ_2 become pure states in the limit of high kinetic energy or low field $(x\to\infty)$. However, as can be observed from the behavior of weight factors a_{ij} $(i,j=1,2)$ for low values of the parameter x, these states are strongly mixed once the values of both components are of the same magnitude. Those important differences between eigenstates Ψ_i $(i=1,2)$ and Ψ_j $(j=3,4)$, as a function of the parameter x, will play an important role in determining the contributions of each resonant transition in the different scattering configurations. In the following discussions through the paper, the character of the valence-band state will be understood as its behavior for $x\to\infty$.

III. SCATTERING AMPLITUDE

The matrix element for the electron-radiation interaction Hamiltonian is given by[2,3]

$$\langle\beta|\hat{H}_{E-R}|I\rangle=\frac{e}{m_0}\sqrt{\frac{2\pi\hbar}{\eta^2\omega V}}\,\mathbf{e}\langle C|e^{i\kappa\cdot\mathbf{r}}\,\mathbf{P}|\Psi\rangle\ , \tag{9}$$

where κ represents the photon wave vector, $\mathbf{e}$ is the polarization of light, η is the refractive index of the crystal, V is the crystal volume, $\mathbf{P}$ is the momentum operator, $|I\rangle$ ($|\beta\rangle$) is the initial (intermediate) state of the system, and $|C\rangle$ ($|\Psi\rangle$) is the electron (hole) wave function in the conduction (valence) band.

According to the Hamiltonian model presented above, the matrix element for the electron-hole pair to phonon interaction via the Fröhlich Hamiltonian is[11]

$$\begin{aligned}\langle\beta|\hat{H}_{E-P}|\alpha\rangle&=\frac{C_F^*}{q}\,\frac{1}{\sqrt{V}}[\,\delta_{N'_{h_j},N_{h_i}}\delta_{\mathbf{K}_h,\mathbf{K}'_h}\delta_{\mathbf{K}'_e,\mathbf{K}_e-\mathbf{q}}\langle C'|C\rangle\\&\times\exp(-iq_xx_{0_e})\,f_{N'_e,N_e}(\lambda^2q_x,x_{0_e}-x'_{0_e})\,\delta_{i,j}\\&-\delta_{N'_e,N_e}\delta_{\mathbf{K}_e,\mathbf{K}'_e}\delta_{\mathbf{K}'_h,\mathbf{K}_h-\mathbf{q}}\cdot\langle\Psi_j^v(\mathbf{K}'_h)|\Psi_i^v(\mathbf{K}_h)\rangle\\&\times\exp(-iq_xx_{0_h})f_{N'_{h_j},N_{h_i}}(\lambda^2q_x,x_{0_h}-x'_{0_h})].\end{aligned} \tag{10}$$

Here $\mathbf{K}_{e(h)}=(k_{y_{e(h)}},k_{z_{e(h)}})$ is the electron (hole) wave vector, $C_F=i(2\pi e^2\hbar\omega_{LO}/V)^{1/2}(\epsilon_\infty^{-1}-\epsilon_0^{-1})^{1/2}$, ϵ_0 is the static and ϵ_∞ is the optical dielectric constants for the material, the index $|\alpha\rangle$ refers to the intermediate electron-hole pair states, $\mathbf{q}$ is the phonon wave vector, $\lambda=(\hbar c/B_0e)^{1/2}$ is the magnetic length, and $x_0=-\lambda^2k_y$. Also, the overlap integrals, $f_{N',N}$, are defined as

$$\begin{aligned}f_{N',N}(\lambda^2q_x,x_0-x'_0)&=\int\Phi_{N'}\left(\xi+\frac{x_0-x'_0}{\lambda}\right)\exp(-iq_x\lambda\xi)\,\Phi_N(\xi)\,d\xi,\end{aligned}$$

where Φ_N are the one-dimensional quantum harmonic oscillator functions.

One may see in Eq. (10) that for each hole transition in the valence band there is an electron transition in the conduction band and the final value of the electron-phonon matrix element arises from the difference between both contributions (electron-hole decompensation effect[1]). Regarding the quasimomentum conservation, the phonon wave-vector component q_z along the magnetic field direction is given by

$$q_z=\frac{\eta}{c}(\omega_L+\omega_S). \tag{11}$$

In first-order Raman scattering processes mediated by deformation potential interaction, the value of q_z can be neglected.[2,3] However, due to the forbidden dipole transition character, this is not the case for the electron-phonon Fröhlich interaction.[1]

The Raman scattering amplitude can be written as

$$W_{FI}=\sum_{\alpha,\beta}\frac{\langle F|\hat{H}_{E-R}|\alpha\rangle\langle\alpha|\hat{H}_{E-P}|\beta\rangle\langle\beta|\hat{H}_{E-R}|I\rangle}{(\hbar\omega_S-E_\alpha+i\gamma_\alpha)(\hbar\omega_L-E_\beta+i\gamma_\beta)}, \tag{12}$$

where E_α is the electron-hole pair energy with lifetime broadening γ_α. The scattering amplitude in Eq. (12) is obtained when the Dyson equation is solved for the electron and hole Green's function.[6,7] In this case, the broadening γ, obtained as the imaginary part of the electron (hole) self-energy, depends on the Landau quantum number, magnetic-field strength, and z component of the wave vector, respectively. Different types of interactions can contribute to the electron or hole self-energy. The Fröhlich mechanism will be the dominant one when the carrier has energy larger than the phonon frequency and the emission of a LO phonon is allowed. The magneto-Raman profile is strongly modified whenever the electron-Fröhlich interaction is switched on.

By using Eqs. (9) and (10), Eq. (12) can be expressed as

$$\begin{aligned}W_{FI}(\omega_S,\mathbf{e}_S;\omega_L,\mathbf{e}_L)=\frac{W_0}{q_z}\sum_{i=1}^{4\ \text{and so}}\sum_{N_e,N_h}\int_{-\infty}^{\infty}\sqrt{\frac{\hbar}{2m_0\omega_c}}dk_z\,\frac{1}{[\hbar\omega_L-E_i(k_z,k_z,N_e,N_h)+i\gamma_i]}\\\times\left(\frac{\langle C|\mathbf{e}_S^*\cdot\mathbf{P}|\Psi_i^v(k_z)\rangle\langle\Psi_i^v(k_z)|\mathbf{e}_L\cdot\mathbf{P}|C\rangle}{[\hbar\omega_S-E_i(k_z-q_z,k_z,N_e,N_h)+i\gamma_i]}\right.\\\left.-\sum_{j=1}^{4\ \text{and so}}\frac{\langle C|\mathbf{e}_S^*\cdot\mathbf{P}|\Psi_j^v(k_z-q_z)\rangle\langle\Psi_j^v(k_z-q_z)|\Psi_i^v(k_z)\rangle\langle\Psi_i^v(k_z)|\mathbf{e}_L\cdot\mathbf{P}|C\rangle}{[\hbar\omega_S-E_j(k_z,k_z-q_z,N_e,N_h)+i\gamma_j]}\right),\end{aligned} \tag{13}$$

where

$$W_0=-\left(\frac{e}{m_0}\right)^2\frac{\hbar}{\sqrt{2}\pi}\,\frac{1}{\sqrt{\eta_L\eta_S}}\,\frac{1}{\sqrt{\omega_L\omega_S}}\,\frac{1}{\lambda^3}\,\frac{C_F^*}{\sqrt{V}}$$

and the energies in the denominators are differences calculated as

$$E_i(k_{z_e},k_{z_h},N_e,N_h)=E_C(k_{z_e},N_e)-E_i^v(k_{z_h},N_h),$$

with $i=1,2,3,4$ and so.

In the Luttinger approximation one gets 18 different combinations of transitions in the valence and conduction bands,

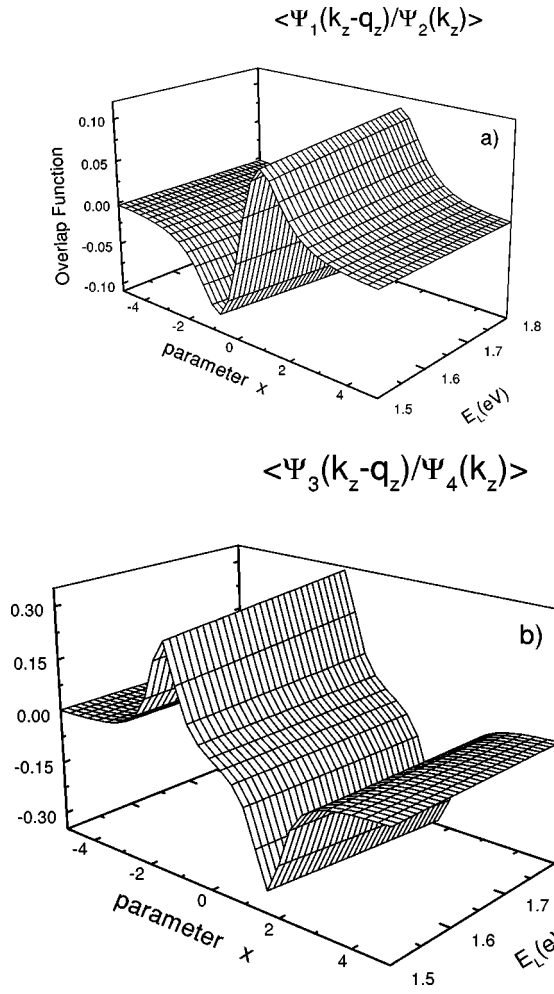

FIG. 2. The overlap functions (a) $\langle\Psi_1(k_z-q_z)|\Psi_2(k_z)\rangle$ and (b) $\langle\Psi_3(k_z-q_z)|\Psi_4(k_z)\rangle$ for GaAs are shown in the energy range of the incident light (1.5–1.8 eV) as a function of the parameter $x=\sqrt{\hbar k_z^2/(2m_0\omega_c)}$ for $B_0=10$ T and Landau quantum number $N=3$. The values of Table I have been used in the calculations and q_z is evaluated according to Eq. (11).

which contribute to the scattering amplitude. Within a parabolic model the allowed ones would be just 6.[2] The allowed transitions between Bloch wave functions at $\mathbf{k}=0$ for each scattering configuration are the following:[2]

$$\begin{aligned}
&\overline{z}(\sigma^+,\sigma^+)z, \qquad \overline{z}(\sigma^-,\sigma^-)z;\\
&\left|\tfrac{3}{2},-\tfrac{3}{2}\right\rangle\rightarrow\left|\tfrac{3}{2},-\tfrac{3}{2}\right\rangle, \quad \left|\tfrac{3}{2},\tfrac{3}{2}\right\rangle\rightarrow\left|\tfrac{3}{2},\tfrac{3}{2}\right\rangle;\\
&\left|\tfrac{3}{2},-\tfrac{1}{2}\right\rangle\rightarrow\left|\tfrac{3}{2},-\tfrac{1}{2}\right\rangle, \quad \left|\tfrac{3}{2},\tfrac{1}{2}\right\rangle\rightarrow\left|\tfrac{3}{2},\tfrac{1}{2}\right\rangle;\\
&\left|\tfrac{1}{2},-\tfrac{1}{2}\right\rangle\rightarrow\left|\tfrac{1}{2},-\tfrac{1}{2}\right\rangle, \quad \left|\tfrac{1}{2},\tfrac{1}{2}\right\rangle\rightarrow\left|\tfrac{3}{2},\tfrac{1}{2}\right\rangle. \qquad (14)
\end{aligned}$$

It can be seen from Eq. (14) that, within a three-band parabolic model, intraband transitions are the only ones allowed. However, by analyzing Eq. (13) for $\mathbf{q}\neq 0$, it can be seen that the products

$$\langle\Psi_j^v(\mathbf{K}_h-\mathbf{q})|\Psi_i^v(\mathbf{K}_h)\rangle \qquad (15)$$

will not vanish even for $i\neq j$ due to the behavior of the wave functions (5)–(8) and the dependences of the weight coefficients a_{ij} on k_z (see Fig. 1). Therefore, there are new terms corresponding to interband transitions that must be considered in the scattering amplitude. In this way the valence-band mixing provides the necessary conditions for the existence of double resonances [see Eq. (13)], which take place once the phonon-assisted transitions occur between bands with different effective masses.[2,12] Due to the smaller $\mathbf{q}$ wave vector the contribution to the Raman intensity from two different valence-band wave functions, evaluated at different values of the hole wave vector shifted at the phonon momentum, is very small if compared to that coming from the mixing factors $|a_{ij}|^2$ in the range $0<x<5$. Figure 2 show a three-dimensional picture of the overlap functions, $\langle\Psi_1(k_z-q_z)|\Psi_2(k_z)\rangle$ and $\langle\Psi_3(k_z-q_z)|\Psi_4(k_z)\rangle$ for $B_0=10$ T and $N=3$, as a function of the dimensionless parameter x, for the energy range of the incident light considered in our study (1.5–1.8 eV). The contribution of those terms to the scattering amplitude is small if compared to that coming from the square weight factors $|a_{ij}|^2$ (see Figs. 1 and 3). Hence the matrix elements responsible for double resonances can be neglected in first-order approximation. Thus, only intraband transitions need to be considered in the Raman process and the scattering amplitude in the $\overline{z}(\sigma^+,\sigma^+)z$ geometry takes the form

$$\begin{aligned}
W_{FI}=\frac{W_0|P|^2}{q_z}\sum_N\int_{-\infty}^{\infty}\sqrt{\frac{\hbar}{2m_0\omega_c}}dk_z\Bigg\{&\frac{2/3}{[\hbar\omega_L-E_{so}^+(k_z,k_z,N,N)+i\gamma_{so}^+]}\Bigg[\frac{1}{[\hbar\omega_S-E_{so}^+(k_z-q_z,k_z,N,N)+i\gamma_{so}^+]}\\
&-\frac{1}{[\hbar\omega_S-E_{so}^+(k_z,k_z-q_z,N,N)+i\gamma_{so}^+]}\Bigg]+\sum_{i=1}^{2}\frac{1/3|a_{2i}(N)|^2}{[\hbar\omega_L-E_i^+(k_z,k_z,N,N)+i\gamma_i^+]}\Bigg[\frac{1}{[\hbar\omega_S-E_i^+(k_z-q_z,k_z,N,N)+i\gamma_i^+]}\\
&-\frac{1}{[\hbar\omega_S-E_i^+(k_z,k_z-q_z,N,N)+i\gamma_i^+]}\Bigg]+\sum_{i=3}^{4}\frac{|a_{2i}(N)|^2}{[\hbar\omega_L-E_i^-(k_z,k_z,N,N)+i\gamma_i^-]}\Bigg[\frac{1}{[\hbar\omega_S-E_i^-(k_z-q_z,k_z,N,N)+i\gamma_i^-]}\\
&-\frac{1}{[\hbar\omega_S-E_i^-(k_z,k_z-q_z,N,N)+i\gamma_i^-]}\Bigg]\Bigg\}. \qquad (16)
\end{aligned}$$

While the expression for the $\overline{z}(\sigma^-,\sigma^-)z$ configuration is the following:

$$W_{FI}=\frac{W_0|P|^2}{q_z}\sum_N \int_{-\infty}^{\infty}\sqrt{\frac{\hbar}{2m_0\omega_c}}dk_z\Bigg\{\frac{2/3}{[\hbar\omega_L-E_{so}^-(k_z,k_z,N,N)+i\gamma_{so}^-]}\Bigg[\frac{1}{[\hbar\omega_S-E_{so}^-(k_z-q_z,k_z,N,N)+i\gamma_{so}^-]}$$
$$-\frac{1}{[\hbar\omega_S-E_{so}^-(k_z,k_z-q_z,N,N)+i\gamma_{so}^-]}\Bigg]+\sum_{i=3}^{4}\frac{1/3|a_{1i}(N+2)|^2}{[\hbar\omega_L-E_i^-(k_z,k_z,N,N+2)+i\gamma_i^-]}$$
$$\times\Bigg[\frac{1}{[\hbar\omega_S-E_i^-(k_z-q_z,k_z,N,N+2)+i\gamma_i^-]}-\frac{1}{[\hbar\omega_S-E_i^-(k_z,k_z-q_z,N,N+2)+i\gamma_i^-]}\Bigg]$$
$$+\sum_{i=1}^{2}\frac{|a_{1i}(N+2)|^2}{[\hbar\omega_L-E_i^+(k_z,k_z-q_z,N,N+2)+i\gamma_i^+]}\Bigg[\frac{1}{[\hbar\omega_S-E_i^+(k_z-q_z,k_z,N,N+2)+i\gamma_i^+]}$$
$$-\frac{1}{[\hbar\omega_S-E_i^+(k_z,k_z-q_z,N,N+2)+i\gamma_i^+]}\Bigg]\Bigg\}. \tag{17}$$

In the above equations the symbols $(\pm)$ in the energy E and lifetime broadening γ correspond to the two different electron spin orientation in the conduction band.

To calculate the one-phonon Raman efficiency[2] one simply replaces expression (16) or (17) into the following equation

$$\frac{dS}{d\Omega}=\left[\frac{\omega_L\omega_S^3\eta_L\eta_S^3}{(2\pi c^2)^2}\right]\left(\frac{V}{(\hbar\omega_L)^2}\right)|W_{FI}(\omega_S,\mathbf{e}_S;\omega_L,\mathbf{e}_L)|^2. \tag{18}$$

IV. DISCUSSION

A direct calculation of the energy broadening, $\gamma_{N_eN_h}(k_e,k_h,B)$, due to electron-phonon Fröhlich interaction is included in the expressions for the Raman efficiency. Even at very low temperature, different processes may contribute to the lifetime broadening enhancement of the electronic intermediate states. Moreover, in a magnetic field when $E_i(k,N)>\hbar\omega_{LO}$ the possibility of resonant coupling between different intraband states, via one LO-phonon emission, becomes real. This effect may strongly contribute to the enhancement of the energy-state broadening. In Refs. 6 and 13 the electron (hole) imaginary part of the self-energy, $\gamma_{N_e}(k_e)[\gamma_{N_h}(k_h)]$, determined by the electron–LO-phonon interaction, was calculated as a function of the electron (hole) wave vector and Landau-level index. In the framework of the noncorrelated electron-hole pair approach, the energy broadening may be written as

$$\gamma_{N_eN_h}(k_e,k_h)=\gamma_{N_e}(k_e)+\gamma_{N_h}(k_h). \tag{19}$$

In this case no valence-band mixing has been considered for the calculation of the hole energy broadening. The results for the energy broadening $\gamma_{33}(k,k)$, in units of $\gamma_o=\hbar\omega_c$, for the case of hh and lh states are shown in Fig. 3. It can be seen that the maxima of the curves are found at $x^2=\omega_{LO}/\omega_c+(N'-N)$, with $N=3$ and $(N'=0,1,2,\ldots,15)$. If $[x^2+(N+1/2)]\leqslant\omega_{LO}/\omega_c$ the electron–LO-phonon interaction is switched off from energy conservation. In this case other interactions may prevail such as the electron-acoustic phonons and/or electron-lattice impurities. Notice that the energy broadening increases as N increases because the probability for phonon-assisted transitions to lower levels rises, that is, $\gamma_{N_1N_1}>\gamma_{N_2N_2}$ for $N_1>N_2$. The scattering rate for the electron–light-hole pair is larger than the electron–heavy-hole pair, due to the expected smaller effective mass of the former carrier. The combined effect of lifetime broadening and the valence-band mixing are relevant to the understanding of the magneto-Raman profile data, as will be discussed next.[14]

In the case of one-phonon Raman scattering assisted by Fröhlich interaction the outgoing resonances are stronger than the incoming ones, once energetically allowed by energy conservation. In Fig. 4, this effect can be appreciated since all resonances are due to outgoing transitions in both parallel scattering geometries. For low enough energies $(\hbar\omega_L<E_g+\hbar\omega_{LO})$ their chance for incoming resonances to be observed in the Raman spectrum increases, once the outgoing resonances are energetically forbidden.

Now we will comment on the principal features observed in the magneto-Raman profile calculations as presented in Fig. 4. As discussed in the deformation potential case,[3] the new transitions appearing in the one-phonon Raman scattering assisted by the Fröhlich interaction cannot be found within a three-band parabolic model. For instance, in the $\overline{z(\sigma^+,\sigma^+)z}$ configuration [see Eq. (16)] the contributions coming from the $a_{22}|\mathrm{lh}^-\rangle$ intraband transitions will not appear in the limit $x\rightarrow\infty$ (parabolic limit) and remain just those produced by the $a_{21}|\mathrm{lh}^-\rangle$ components. The component $a_{22}|\mathrm{lh}^-\rangle$ of the state Ψ_2, which has hh^+ character, is suppressed at high energies and/or low values of the magnetic field. For relatively low energies (or high magnetic field) the transitions with the weight coefficients a_{22} are the strongest ones [see Figs. 1 and 4(a)]. Furthermore, in this scattering geometry and at low energies, another strong resonance could be expected from those transitions originated from the components $a_{23}|\mathrm{hh}^-\rangle$ of Ψ_3, which has lh^+ character. Those components would also be strong for low values of the parameter x, however, due to their light-hole character and to the relatively higher energy broadening (small effective

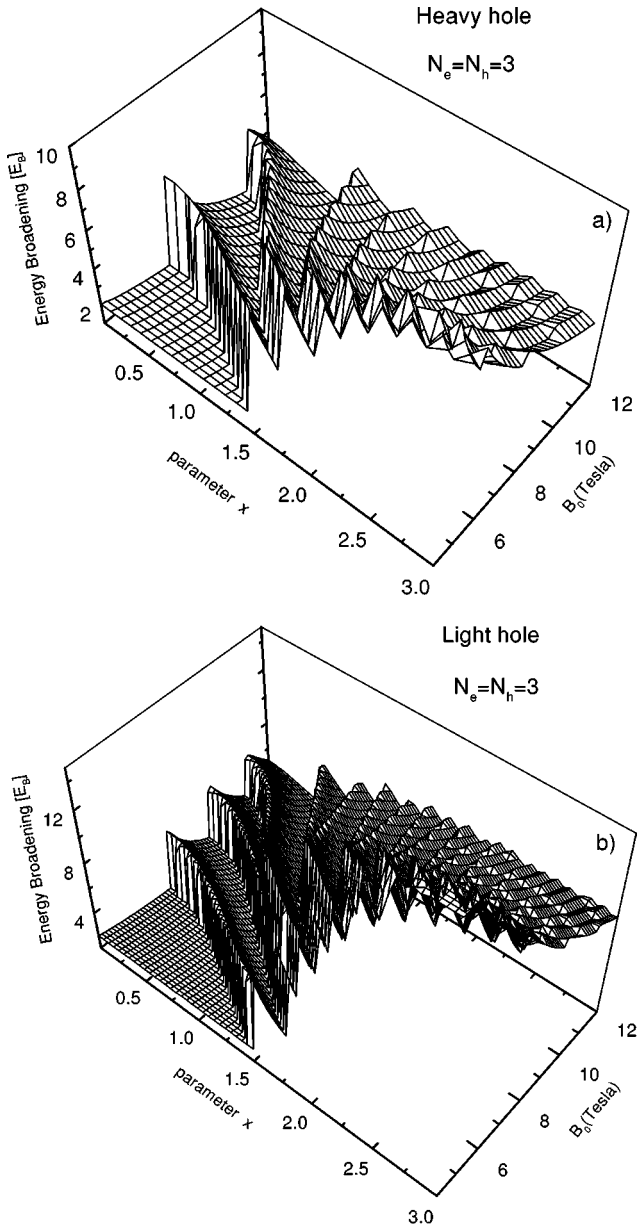

FIG. 3. The 3D picture of the energy broadening of an electron-hole pair, $\gamma_{33}(k,k)$, in units of $\gamma_o=\hbar\omega_c$ [$E_B=\gamma_{33}(k,k)/\gamma_o$], as a function of the parameter x and the magnetic-field strength B_0. (a) Heavy-hole contribution. (b) light-hole contribution. For the calculations the values listed in Table I have been used.

mass, see Fig. 3), their corresponding Raman intensities will be strongly reduced. The other states that show heavy-hole character and small energy broadening, as can be seen in Fig. 1, are those with components $a_{24}|\mathrm{hh}^-\rangle$ (from state Ψ_4). Nevertheless, there are large differences between the dependence of the coefficients a_{22} and a_{24} for low values of x and thus the states with components a_{24} will only be relevant at high energies. Moreover, the transitions between $a_{24}|\mathrm{hh}^-\rangle$ components become the strongest ones for energies above 1680 meV, as can be seen in Fig. 4(b).

There is another interesting effect associated with the strong valence-band mixing that produces qualitative differences between the Raman spectra in both parallel scattering geometries. Notice that, in the case of the $\overline{z}(\sigma^-,\sigma^-)z$ configuration [see Eq. (17)], the relevant transitions at low energies [see Fig. 4(c)] are those produced from the components $a_{14}|\mathrm{lh}^+\rangle$, of state Ψ_4 with hh^- character (see Fig. 1). Now, at high energies, and according to the dependence of coefficients a_{14} and a_{12} on the parameter x, the relevant transitions are those due to the components $a_{12}|\mathrm{hh}^+\rangle$, of state Ψ_2. At this point the situation is similar to the $\overline{z}(\sigma^+,\sigma^+)z$ configuration [compare Figs. 4(b) and 4(d)]. However, in $\overline{z}(\sigma^-,\sigma^-)z$ scattering geometry there are transitions between $a_{12}|\mathrm{hh}^+\rangle$ components that can be also seen, even at relatively low energies [Fig. 4(c)], together with those produced from the $a_{14}|\mathrm{lh}^+\rangle$ ones. Note that the states Ψ_2 and Ψ_4 present heavy-hole character and, therefore, the corresponding energy broadening is small [see Fig. 3(a)]. The same happens to the components $a_{24}|\mathrm{hh}^-\rangle$ in the $\overline{z}(\sigma^+,\sigma^+)z$ geometry. However, the different behavior of the coefficients a_{24} and a_{12} at low values of x determines that the Raman intensity coming from the $a_{24}|\mathrm{hh}^-\rangle$ component is negligible. Moreover, for high energy the main resonances in the $\overline{z}(\sigma^+,\sigma^+)z$ geometry come from the $a_{24}|\mathrm{hh}^-\rangle$ state [see Fig. 1 and compare Figs. 4(a) and 4(c)], leaving unaffected, in the $\overline{z}(\sigma^-,\sigma^-)z$ configuration, those from $a_{12}|\mathrm{hh}^+\rangle$. Therefore, spectra in the $\overline{z}(\sigma^+,\sigma^+)z$ scattering geometry present less valence-band mixing, at low energies, than those in the $\overline{z}(\sigma^-,\sigma^-)z$ geometry. In this way, the valence-band admixture helps to explain experimental observations for Raman intensity in GaAs, as reported in Ref. 14.

TABLE I. GaAs parameters used for the calculations.

$E_g=1519$ meV[a]	$\Delta_0=341$ meV[a]	$\hbar\omega_{LO}=37$ meV[a]
$\gamma_1=6.85$[a]	$q_{LK}=0$	$\epsilon_0=12.5$[a]
$\gamma_2=2.1$[a]	$\eta=3.346$[a]	$\epsilon_\infty=10.9$[a]
$\gamma_3=2.9$[a]	$m_c=0.0665m_0$[a]	$g_c=-0.32$[b]
$\kappa=1.2$[a]	$m_{so}=0.170m_0$[a]	$g_{so}=4.5$[b]

[a]From Ref. 17.
[b]From Ref. 2.

The excitonic corrections to the energy Landau levels have also been included in all calculations making use of the high-field limit as reported in Ref. 15. The excitonic binding energy, which depends on the Landau-level index and the magnetic-field strength, causes a redshift of the Raman resonances for high values of the magnetic field. Note that the excitonic effects on the electronic states were not included in the scattering amplitude. Due to the high value of the exciton oscillator strength, this effect is relevant for absolute values of the Raman intensities.[16] In this sense, our comparison with experimental magneto-Raman intensities are valid in relative units.

In Figs. 4(a)–4(d) we compare the calculated Raman efficiencies, which include excitonic corrections to the experimental results reported in Ref. 14 and see that the overall agreement is quite good. Notice, in Fig. 4(a), the shoulder in the experimental peak near $B_0=10.8$ T at incident energy $E_L=1640$ meV. It is our understanding that this shoulder might correspond to the resonant polaron coupling between Landau levels $N=4$ and $N=2$ in the conduction band of GaAs crystals. In order to verify it we have introduced, in the Raman efficiency calculation, the renormalization of the conduction Landau levels through the magnetopolaron self-

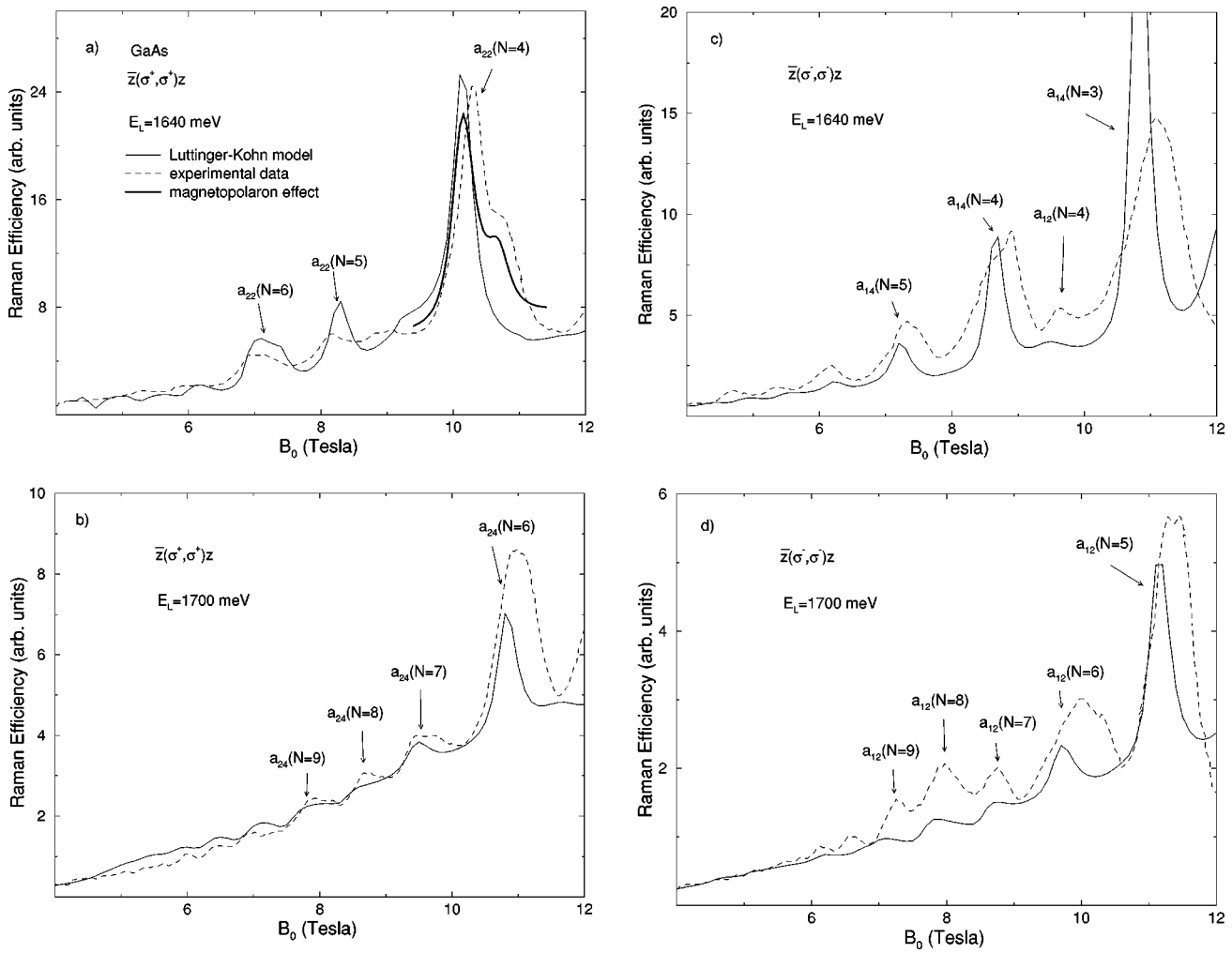

FIG. 4. Calculated Raman intensity in bulk GaAs as a function of the magnetic field for different energies of the incident light ($E_L = \hbar\omega_L$) for the scattering geometry $\overline{z}(\sigma^+,\sigma^+)z$, (a) $E_L = 1640$ meV, (b) $E_L = 1700$ meV; and the $\overline{z}(\sigma^-,\sigma^-)z$ configuration, (c) $E_L = 1640$ meV, (d) $E_L = 1700$ meV. The solid thin lines correspond to the theoretical results. The dashed lines are the experimental data and the solid dark line at the graphic (a) is the result due to the magnetopolaron effect on the conduction band. In all calculations we have used the values listed in Table I.

energy using the results reported in Ref. 5. The calculated magnetopolaron resonance is shown in the thicker solid line of Fig. 4(a) and gives strong support to our predictions. Furthermore, due to the high effective mass of the heavy-hole carrier this effect may be very small in the valence band because the coupling will take place between states of high Landau-level index and so the magnetopolaron resonances will be very broadened and weak. The theoretical results for the Raman efficiency, calculated within our Hamiltonian model and including both excitonic and magnetopolaron effects, reproduce quite well the shoulder of the corresponding experimental resonant peak near $B_0 = 10.8$ T.

The last effect that we observe in the magneto-Raman intensity is an induced band nonparabolicity. In simple three band parabolic model the effective masses are independent of the magnetic field[2] and thus the peak positions in the magneto-Raman profile will be proportional to the applied field. The above is no longer true in the present Hamiltonian model and this mass-induced nonparabolicity can be clearly seen in Figs. 4(a)–4(d).

V. CONCLUSIONS

The model, which takes the valence-band mixing into account, shows resonant features that could not be predicted using a simple three-band parabolic model. Conditions for double resonances within the framework of Fröhlich interaction are satisfied once the band admixture is considered. This happens since new interband transitions, that are forbidden in a three-band parabolic model, will become allowed. This effect was neglected in the calculation of the scattering amplitude due to the small values for the magnitude of the involved phonon wave vector.

The band mixing and the induced mass nonparabolicity have relevant effects in the case of Raman scattering assisted by Fröhlich interaction and produce some evident differences between the two scattering configurations with parallel geometries $\overline{z}(\sigma^+,\sigma^+)z$ and $\overline{z}(\sigma^-,\sigma^-)z$. For low laser energy or high magnetic field the Raman spectra for the $\overline{z}(\sigma^+,\sigma^+)z$ configuration appears to be ''cleaner'' from different contributions because the interference between different intraband

transitions is strongly reduced [see Figs. 4(a) and 4(c)]. However, for higher energies the parabolic limit is recovered and both spectra show sharp peaks due to just one kind of intraband transition.

The lifetime broadening calculations combined with the effect of the valence-band mixing yield a better understanding of the experimental results and confirm the strong effect of the electron-phonon Fröhlich interaction on the enhancement of the energy indetermination of these Landau states. The sharp resonances observed in the magneto-Raman scattering allow a clear identification of polaron effects on the electronic band structure, as was confirmed by introducing the magnetopolaron self-energy in the renormalization of the conduction-band Landau levels.

ACKNOWLEDGMENTS

V.L. acknowledges FAPESP for financial support of this work. G.E.M. acknowledges CNPq for partial financial support. The authors are indebted to T. Ruf, who provided the experimental data used in this work.

*Also at Departamento de Física Teórica, Universidad de La Habana, 10400 C. Habana, Cuba.

[1] M. Cardona, in *Light Scattering in Solids II*, edited by M. Cardona and G. Güntherodl, Topics in Applied Physics, Vol. 50 (Springer-Verlag, Heidelberg, 1982), p. 19.

[2] C. Trallero-Giner, T. Ruf, and M. Cardona, Phys. Rev. B **41**, 3028 (1990).

[3] V. López, G. E. Marques, J. Drake, and C. Trallero-Giner, Phys. Rev. B **56**, 15 691 (1997).

[4] T. Ruf, R. T. Phillips, C. Trallero-Giner, and M. Cardona, Phys. Rev. B **41**, 3039 (1990).

[5] V. López, F. Comas, C. Trallero-Giner, T. Ruf, and M. Cardona, Phys. Rev. B **54**, 10 502 (1996).

[6] V. I. Belitsky, C. Trallero-Giner, and M. Cardona, Phys. Rev. B **48**, 17 861 (1993).

[7] V. I. Belitsky, C. Trallero-Giner, and M. Cardona, Phys. Rev. B **49**, 11 016 (1994).

[8] J. M. Luttinger and W. Kohn, Phys. Rev. **97**, 869 (1955).

[9] J. M. Luttinger, Phys. Rev. **102**, 1030 (1956).

[10] M. H. Weiller, in *Magneto Optical Properties of* $Hg_{1-x}Cd_xTe$ *Alloys*, edited by R. K. Willardson and A. C. Beer, Semiconductors and Semimetals, Vol. 16 (Academic, New York, 1966).

[11] A. K. Ganguly and J. L. Birman, Phys. Rev. **162**, 806 (1967).

[12] The existence of double resonances in parallel scattering configurations was pointed out for the first time, to our knowledge, by G. C. La Rocca, T. Ruf, and M. Cardona, Phys. Rev. B **41**, 12 672 (1990).

[13] C. Trallero-Giner, F. Iikawa, and M. Cardona, Phys. Rev. B **44**, 12 815 (1991).

[14] T. Ruf, Ph.D. thesis, Max-Planck-Institut für Festkörperforschung, Stuttgart, 1990.

[15] T. Ruf, R. T. Phillips, A. Cantarero, G. Ambrazeviçius, M. Cardona, J. Schmitz, and U. Rössler, Phys. Rev. B **39**, 13 378 (1989).

[16] A. Cantarero, C. Trallero-Giner, and M. Cardona, Phys. Rev. B **39**, 8388 (1989).

[17] *Physics of Group IV Elements and III-V Compounds*, edited by O. Madelung, M. Schultz, and H. Weiss, Landolt-Börnstein, New Series, Group III, Vol. 17, Pt. a (Springer-Verlag, Berlin, 1982).